



Current driven chiral domain wall motions in synthetic antiferromagnets with Co/Rh/Co

Cite as: J. Appl. Phys. **128**, 053902 (2020); <https://doi.org/10.1063/5.0012453>

Submitted: 01 May 2020 . Accepted: 16 July 2020 . Published Online: 03 August 2020

Alexander Cohen , Alexis Jonville, Zhentao Liu, Chirag Garg, Panagiotis Ch. Filippou, and See-Hun Yang 

COLLECTIONS

Paper published as part of the special topic on [Antiferromagnetic Spintronics](#)



View Online



Export Citation



CrossMark

ARTICLES YOU MAY BE INTERESTED IN

[Electrical readout of the antiferromagnetic state of IrMn through anomalous Hall effect](#)
Journal of Applied Physics **128**, 053904 (2020); <https://doi.org/10.1063/5.0009553>

[Spintronics with compensated ferrimagnets](#)

Applied Physics Letters **116**, 110501 (2020); <https://doi.org/10.1063/1.5144076>

[Study of the perpendicular magnetic anisotropy, spin-orbit torque, and Dzyaloshinskii-Moriya interaction in the heavy metal/CoFeB bilayers with Ir₂₂Mn₇₈ insertion](#)

Applied Physics Letters **116**, 242407 (2020); <https://doi.org/10.1063/5.0006138>

Lock-in Amplifiers
up to 600 MHz



Current driven chiral domain wall motions in synthetic antiferromagnets with Co/Rh/Co

Cite as: J. Appl. Phys. 128, 053902 (2020); doi: 10.1063/5.0012453

Submitted: 1 May 2020 · Accepted: 16 July 2020 ·

Published Online: 3 August 2020



Alexander Cohen,^{1,2} Alexis Jonville,^{1,3} Zhentao Liu,^{1,4} Chirag Garg,¹ Panagiotis Ch. Filippou,¹ and See-Hun Yang^{1,a)}

AFFILIATIONS

¹IBM Research—Almaden, San Jose, California 95120, USA

²The Pritzker School of Molecular Engineering, University of Chicago, Chicago, Illinois 60637, USA

³École supérieure de physique et de chimie industrielles de la Ville de Paris, Paris 75005, France

⁴Department of Electrical and Electronic Engineering, École Polytechnique Fédérale de Lausanne, 1015 Lausanne, Switzerland

Note: This paper is part of the special topic on Antiferromagnetic Spintronics.

a) Author to whom correspondence should be addressed: seeyang@us.ibm.com

ABSTRACT

Spin-orbit torque that originates from spin Hall effect and Dzyaloshinskii–Moriya interaction (DMI) can efficiently move chiral magnetic domain walls in perpendicularly magnetized wires. It has been shown that antiferromagnetically coupled composite domain walls across a ruthenium layer can be driven even faster by exchange coupling torque that is proportional to exchange coupling strength. Here, we report a current-driven motion of composite chiral domain walls in synthetic antiferromagnets with a rhodium spacer layer. It is found that the domain walls in the wire with a rhodium layer do not move as fast as that with a ruthenium layer although the exchange coupling in Co|Rh|Co is stronger than Co|Ru|Co, which is due to the formation of a large DMI at the Rh|Co interface. The Dzyaloshinskii–Moriya interaction at the Co/Rh interface has the same sign and comparable strength to the Pt|Co interface, thus negating the exchange coupling torque. The spin Hall effect from rhodium is found to be as small as ruthenium. Our findings show that rhodium can be used to tailor the DMI strengths in the current-driven motion of chiral domain walls in various magnetic nanostructures.

Published under license by AIP Publishing. <https://doi.org/10.1063/5.0012453>

I. INTRODUCTION

Spin transfer torque to move magnetic domain walls (DWs) by current in nanowires opens the door to a potential development of logic or storage class memories such as racetrack memory.^{1,2} Such devices encode data bits in magnetic domains that can be accessed by moving DWs via current pulses along the wire instead of mechanical motion.³ The data encoded in domains are read out by, e.g., tunneling magnetoresistance through magnetic tunnel junctions. Note that the higher DW mobility allows faster devices since the data access time is determined by the DW velocity.

There are three types of torques that drive DWs by current: conventional volume spin transfer torque (STT),⁴ spin-orbit torque (SOT),^{5,6} and exchange coupling torque (ECT).^{7–9} The STT is caused by the spin current inside the magnetic metallic wire due to spin-dependent scattering of spins by magnetic moments. In the STT, angular momenta are reciprocally transferred between spins

and magnetic moments in DWs under the angular momentum conservation, thus driving DWs along electron flow direction in conventional magnetic metal wires. The DWs typically move up to 100–150 m/s by STT at a current density $J \sim 10^8$ A/cm².^{10,11} On the other hand, the SOT is formed from both spin Hall effect (SHE)^{12,13} and Dzyaloshinskii–Moriya interaction (DMI).^{14,15} Here, the SHE generates a spin current from the heavy metal layer that interfaces with the magnetic wire,¹⁶ while the DMI plays a key role in the formation of chiral Néel-type walls.¹⁷ A broken inversion symmetry at a heavy metal/ferromagnetic interface gives rise to the interface DMI that produces a local DMI field thus stabilizing the Néel-type walls. The chiral DWs are moved by this local DMI field with the assistance of SHE induced spin current.¹⁸ The SOT alone in the ferromagnetic wire can drive the DWs more efficiently than STT by more than 2–3 times.¹⁹ Distinctly from the STT, the DWs can be moved along either current or electron flow direction depending on the signs of SHE and DMI. However,

despite high efficiency of SOT, large stray fields around packed DWs and DW tilting potentially limits the increase of density in chips.²

The ECTs that were discovered from DWs in synthetic antiferromagnetic (SAF) and ferrimagnetic wires are even more efficient than the SOT.⁷ Notably, the ECTs increase as the net magnetizations decrease such that the DW velocity forms a maximum at fully compensated magnetization, thus possibly exceeding 1 km/s in fully compensated SAF⁷ and a few km/s in nearly compensated ferrimagnets.^{20–22} The main driving forces in the ECTs to move DWs are the exchange coupling field and the SHE induced spin current, thus leading to increased DW velocity with the increasing exchange coupling strength and spin current. In particular, the composite DWs in synthetic antiferromagnetic wires are promising since (a) magnetic tunnel junction for tunneling magnetoresistance can be readily integrated for readout, (b) the DWs are insensitive to geometric effect due to small DW tilting, and (c) stray fields can be minimized, thus allowing the development of denser chips. The SAF wires are typically formed from two perpendicularly magnetized layers (e.g., Co|Ni|Co) that are separated by a spacer layer like ruthenium.⁷ The exchange coupling is induced by the Ruderman–Kittel–Kasuya–Yosida (RKKY) interaction, thus leading to oscillatory sign and exponential decay of strength in exchange coupling as a function of the spacer layer thickness.^{23,24} Since the exchange coupling field across a ruthenium spacer can be significantly larger than the DMI field, much more efficient DW velocity is allowed.

In this paper, we present current-driven DW motion in SAF wires with a rhodium spacer layer. Since rhodium is known to have a larger exchange coupling strength ($J^{\text{ex}} \sim -1.6 \text{ erg cm}^{-2}$ at $t_{\text{Rh}} = 7 \text{ \AA}$)²⁵ than ruthenium ($J^{\text{ex}} \sim -0.5 \text{ erg cm}^{-2}$ at $t_{\text{Ru}} = 8 \text{ \AA}$)²⁴ when interfaced with the Co layer, the DW velocity in Rh-based SAF is expected to show higher DW velocity. On the contrary, we find that the SAF wires with a rhodium spacer layer have lower domain wall velocity by current than the counterpart with a ruthenium layer due to a large DMI field at Rh/Co interface that compensates the ECTs. The SHE induced spin current from the Rh layer, on the other hand, is found to be small like the Ru layer.

II. EXPERIMENT

Single and SAF layer films are grown using DC magnetron sputtering deposition. The common underlayers are 100 Al₂O₃|20 TaN|20 Pt on a Si(001)|250 SiO₂ substrate while 50 TaN is commonly used as a capping layer to protect against oxidation of layers underneath. Here, all thicknesses are in Angstrom and hereafter unless otherwise notified. The single-layer stacks are 3 Co|7 Ni|1.5, 3 Co|0, 1, 3, 7, 9, 11, and 13 Rh while the SAF structures are composed of 3 Co|7 Ni|1.5 Co|6, 7, 8, and 9 Rh|3 Co|7 Ni|3 Co. All magnetic films show decent perpendicular magnetic anisotropies (PMAs) exhibiting square easy-axis hysteresis loops that are measured by a superconducting quantum interference device (SQUID) and polar magneto-optic Kerr effect (PMOKE). The wires (2 μm wide and 50 μm long) were patterned from the grown films using photolithography and argon ion beam milling. Polar MOKE microscopy is used to measure the DW velocity by imaging the positions of DWs along the wires in differential contrast mode in response to the application of sequences of 5 ns-long current pulses. Longitudinal magnetic fields up to $\pm 3 \text{ kOe}$ along the wire

direction are applied to measure the DMI local fields. Current densities ranging from -2.5 to $2.5 \times 10^8 \text{ A cm}^{-2}$ are used.

III. RESULTS AND DISCUSSION

The magnetic properties of SAF structure are sensitive to the Rh thickness, t_{Rh} , showing spin-flop behavior as seen from the magnetic hysteresis loops that are measured from blanket films [Fig. 1(a)]. The antiferromagnetic exchange coupling forms a maximum around $t_{\text{Rh}} = 7 \text{ \AA}$ where the saturation field and coercivity are maximized. As expected, the saturation field and exchange coupling across the Rh layer is larger than the Ru counterpart.^{7,23} Current-driven DW motion from the patterned wires shows that the DWs move along the current flow direction [Fig. 1(b)] as previously observed from SOT and ECT driven DW motion in SAF wires based on the Ru spacer layer. As anticipated from Ru-based SAF wires, the DW velocity in the absence of external field increases with the increased exchange coupling strength due to the enhanced ECTs thus showing maximum DW velocity $\sim 550 \text{ m/s}$ at the current density $J = 2.2 \times 10^8 \text{ A/cm}^2$ when $t_{\text{Rh}} = 7 \text{ \AA}$ [Fig. 1(c)]. Note, however, that this value is even smaller than 750 m/s observed from the Ru spacer layer based counterpart,⁷ which is counter-expected since the exchange coupling strength is larger for $t_{\text{Rh}} = 7 \text{ \AA}$ than the SAF with $t_{\text{Rh}} = 8 \text{ \AA}$ as seen from the hysteresis loops.

To understand why the DW velocity in SAF wires with the Rh layer is unexpectedly low, we investigate the single-layer wires that have Rh layers on top of magnetic layers. Here, 3 Co|7 Ni|1.5, and 3 Co as magnetic layers are used to evaluate the effect of two interfaces in the bottom and top on current-driven DW motion while 0, 1, 3, 7, 9, 11, and 13 Rh are grown on top. All the film stacks exhibit excellent PMA (the easy-axis magnetic hysteresis loops are not presented here). The DWs in the wires patterned from these films are found to move along the current flow direction, thus showing that the dominant driving force to move DWs is the SOT [Fig. 2(a)]. Most importantly, note that the DW velocity significantly decreases with the increasing t_{Rh} . This reminds us of the Pt capping layer that reduces the total DMI field and SHE induced spin current.⁵ The signs of DMI fields and spin current at Co|Pt interface is opposite to those at Pt|Co interface due to the anti-symmetrical nature of DMI and SHE against the reflection operation with respect to the film plane. Hence, the significant reduction of DW velocity in wires formed from Co|Ni|Co|Rh suggests that there must exist a large DMI at Co|Rh or a large SHE from the Rh layer or both.

To quantify the DMI field and SHE, the DW velocity v are measured in the presence of longitudinal fields H_x since the value at the point where the $v-H_x$ curve crosses the H_x -axis corresponds to $\sim -H_{\text{DM}}$ while the slope of $v-H_x$ curve is nearly proportional to spin Hall strength H_{SH} when the conventional STT and current density are small. One-dimensional (1D) analytical model is used to analyze the experimental data here.¹⁹ The DMI field is described as $H_{\text{DM}} = \frac{D}{M\Delta}$ where D , M , and Δ are DMI constant, saturation magnetization, and DW width, respectively. The strength of SHE induced spin current is typically parameterized by spin Hall parameter H_{SH} that is given by $H_{\text{SH}} = \frac{\hbar\theta_{\text{SH}}J_{\text{UL}}}{2eM\Delta}$ ($\hbar = \frac{h}{2\pi}$, where h is the Planck constant, θ_{SH} is the effective spin Hall angle for an underlayer like Pt, J_{UL} is the current density for the layer of spin Hall

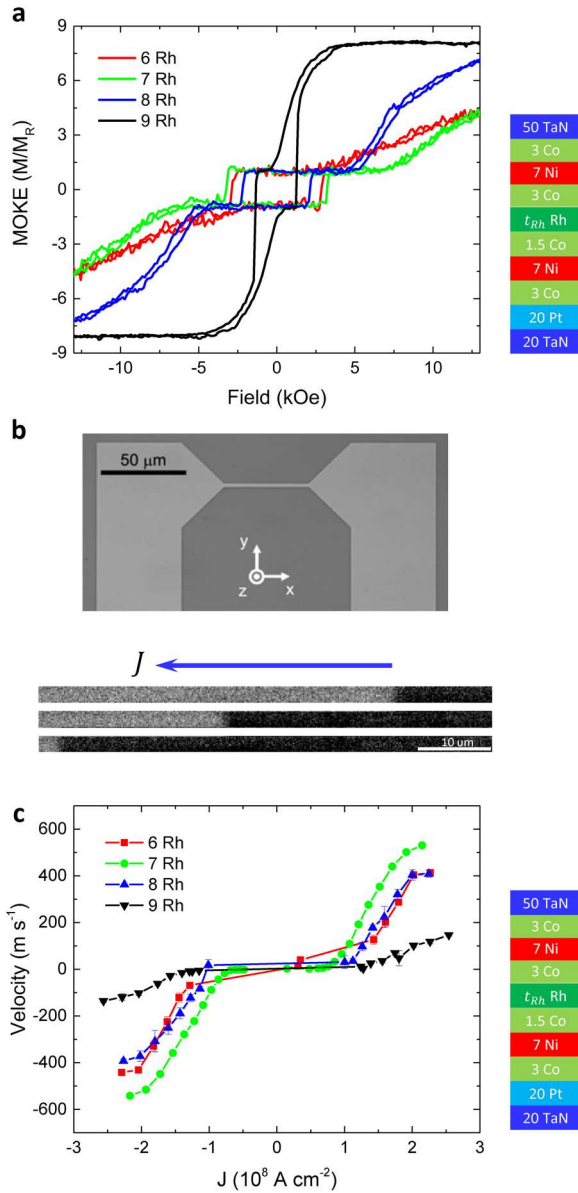


FIG. 1. (a) Easy-axis hysteresis loops measured by polar MOKE that are normalized at the remnant magnetization M_R for various t_{Rh} from 20 TaN|20 Pt|3 Co|7 Ni|1.5 Co| t_{Rh} Rh|3 Co|7 Ni|3 Co. (b) Optical microscope image of the device wire that is 2 μm wide and 40 μm long (upper panel). MOKE image of the SAF wire after a successive few 5 ns-long current pulses. Current density $J = 2.2 \times 10^8$ A/cm² is used here (lower panel). (c) Plot of DW velocity v vs current pulse density J for t_{Rh} = 6 (red), 7 (green), 8 (blue), and 9 Å (black). Error bars are one standard deviation.

current source, e is the electric charge, and t_M is the magnetic layer thickness). The DW width, SHE, and DMI field parameters are obtained by tuning the fitting parameters of the 1D model to the experimental data [solid lines in Figs. 3(a) and 3(b)].

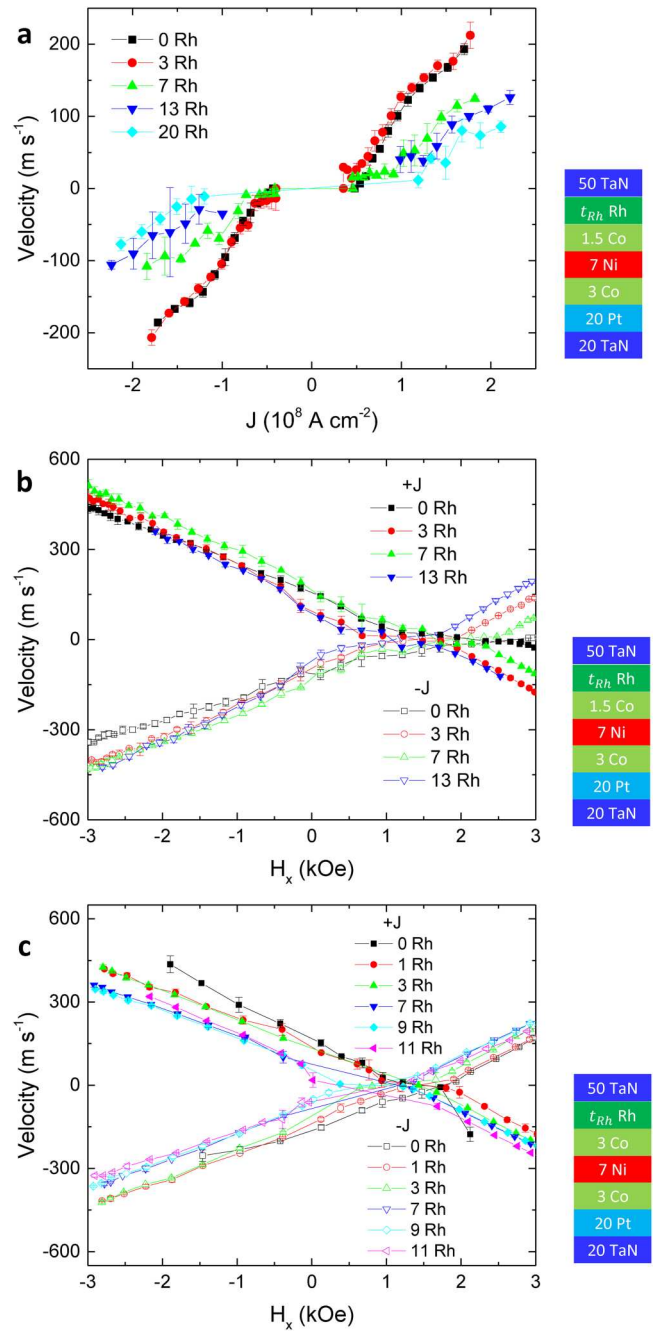


FIG. 2. (a) Plot of DW velocity v vs current pulse density, J , for various t_{Rh} in a single-layer stack structure for 20 TaN|20 Pt|3 Co|7 Ni|1.5 Co| t_{Rh} Rh. (b) Measured DW velocities vs longitudinal field H_x for t_{Rh} = 0 (black), 3 (red), 7 (green), and 13 Å (blue) for 20 TaN|20 Pt|3 Co|7 Ni|1.5 Co| t_{Rh} Rh. (c) Measured DW velocities vs longitudinal field H_x for t_{Rh} = 0 (black), 1 (red), 3 (green), 7 (blue), 9 (cyan), and 11 Å (magenta) for 20 TaN|20 Pt|3 Co|7 Ni|3 Co| t_{Rh} Rh. (b) and (c) Solid and open symbols correspond to the positive and negative J , respectively. Here, $J = 1 \times 10^8$ A/cm² is used. (a)–(c) Error bars correspond to one standard deviation.

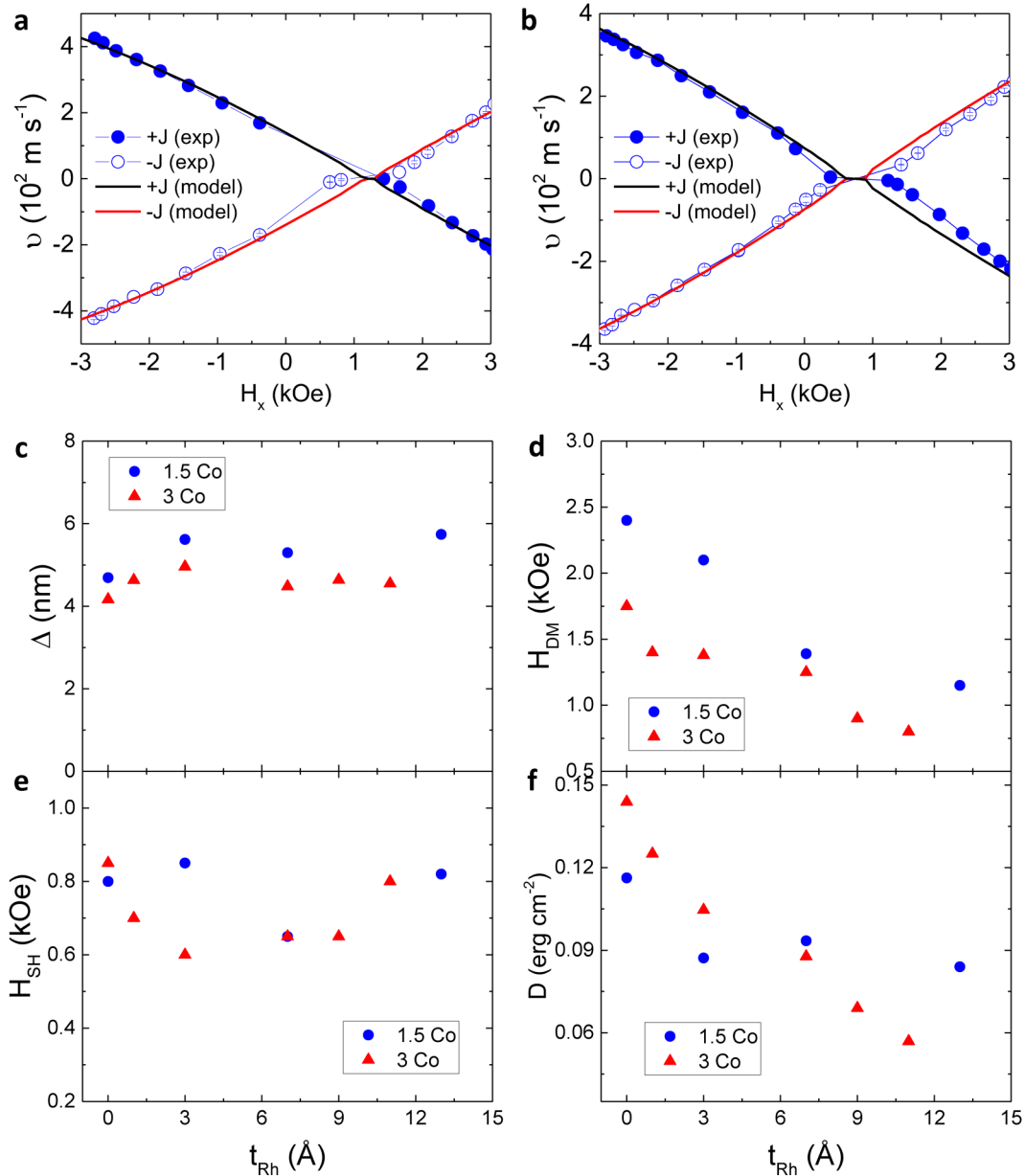


FIG. 3. (a) and (b) Examples of 1D model fitting to the experimental data of 20 Ta|20 Pt|3 Co|7 Ni|3 Co| $t_{\text{Rh}} = 3$ (a), 9 (b) Rh in Fig. 2(c). Plots of (c) DW width parameter Δ , (d) DMI field H_{DM} , (e) SH parameter H_{SH} , and (f) DMI parameter D vs t_{Rh} in wires formed from a single layer (SL) that are fitted to Figs. 2(b) and 2(c) using 1D analytical model. Blue and red symbols correspond to 1.5 Co and 3 Co that interface with a Rh layer on top, respectively. During the fitting, Gilbert damping $\alpha = 0.1$ is used, while volume STT is not considered.

Since the spin Hall strength is associated with the spin diffusion length, the SHE increases with the spin current source layer thickness (here t_{Rh}) and becoming saturated as the layer is thicker than spin diffusion length. Although the DMI is sensitive to the interface, certain thicknesses of two interface layers are required to establish a decent DMI strength.^{5,26} The crossing field of $v-H_x$

curves with H_x axis significantly decreases with Rh thickness with a given interfacing Co thickness suggesting that H_{DM} decreases with the Rh thickness [Fig. 3(d)]. In addition, H_{DM} for $t_{\text{Co}} = 3$ Å is larger than that for $t_{\text{Co}} = 1.5$ Å. Note that the Rh layer on top interfaces with not only the Co layer but also the Ni layer when $t_{\text{Co}} = 1.5$ Å, which is thinner than a monolayer of Co. These

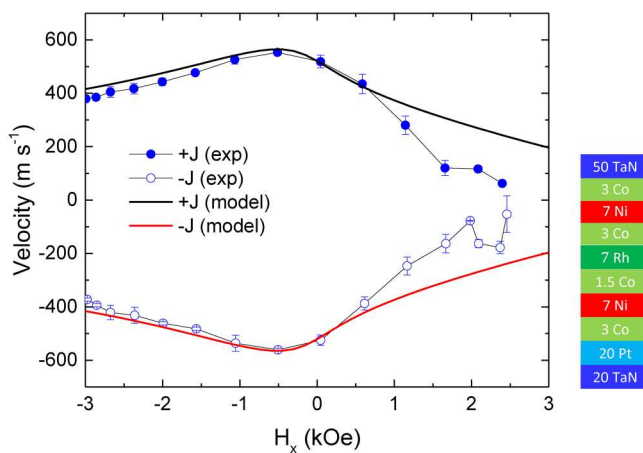


FIG. 4. Measured (blue symbols) and calculated (red curves) DW velocity vs longitudinal field H_x in SAF wires formed from 20 TaN|20 Pt|3 Co|7 Ni|1.5 Co|7 Rh|3 Co|7 Ni|3 Co. Solid (black) and open (red) symbols (curves) correspond to the positive and negative $J = 1.9 \times 10^8$ A/cm², respectively. Fitted parameters are $\Delta = 3.3$ nm, $J^{ex} = -0.28$ erg/cm², $H_{SH} = 1$ kOe (lower layer), $H_{SH} = 0.35$ kOe (upper layer), $H_{DM} = 1.4$ kOe (lower layer), and $H_{DM} = 0.6$ kOe (upper layer). Like a single-layer case in Fig. 3, Gilbert damping $\alpha = 0.1$ is used, while volume STT is not considered.

clearly show that DMI from the upper Co/Rh interface compensates that from the lower Pt/Co interface. It is found from hard-axis magnetization hysteresis loop measurement with SQUID-VSM (the data are not shown here) that the anisotropy K_{eff} and the saturation magnetization M do not change much as a function of t_{Rh} . Consequently, the DW width parameter Δ does not vary much against t_{Rh} and the total DMI constant D significantly decreases with the increasing t_{Rh} [Figs. 3(a) and 3(f)]. On the other hand, the fitted spin Hall parameters H_{SH} using the 1D analytical model exhibit small changes as a function of t_{Rh} [Fig. 3(e)], thus suggesting that the SHE from Rh is small although slightly larger than Ru. The small SHE in Rh is consistent with the tight-binding model.²⁷ As a result, we find that the signs of DMI and SHE at the Co/Rh interface are the same as the Co/Pt interface.

The $v-H_x$ measurements on the Rh-based SAF wire show a characteristic non-monotonic behavior, thus forming a broad maximum (~ 550 m/s) around $H_x = -0.5$ kOe, where the SOT is believed to be minimized while the ECTs becomes maximized. When the parameters that were obtained to fit curves for a single-layer case in Fig. 3 are reused to fit curves for a single-layer case in Fig. 4, the fitted parameters using 1D analytical model^{7,9} show good agreement with each other.

IV. CONCLUSION

We carry out the current-driven DW motion from the wires formed from SAF wires with the Rh spacer layer. We find that the SAF with the Rh spacer layer has a stronger exchange coupling interaction than the Ru spacer layer but DW speeds are significantly smaller than the same system with Ru. We find that this is due to a large DMI field at Co/Rh interface, thus compensating the DMI at Pt/Co interface. This consequently negates the exchange

coupling torque. On the other hand, the SH induced spin current from the Rh layer is comparable to the Ru layer. Our observations show that the Rh layer has the potential to tune the DMI strengths in the current-driven motion of chiral domain walls and skyrmions in magnetic nanostructures.

ACKNOWLEDGMENTS

We thank the Army Research Office (Contract No. W911NF-13-1-0107) for their partial support of this work.

DATA AVAILABILITY

The data that support the findings of this study are available from the corresponding author upon reasonable request.

REFERENCES

- S. S. P. Parkin, M. Hayashi, and L. Thomas, *Science* **320**, 190 (2008).
- S. Parkin and S.-H. Yang, *Nat. Nanotechnol.* **10**, 195 (2015).
- M. Hayashi, L. Thomas, R. Moriya, C. Rettner, and S. S. P. Parkin, *Science* **320**, 209 (2008).
- D. C. Ralph and M. D. Stiles, *J. Magn. Magn. Mater.* **320**, 1190 (2008).
- K.-S. Ryu, L. Thomas, S.-H. Yang, and S. Parkin, *Nat. Nanotechnol.* **8**, 527 (2013).
- S. Emori, U. Bauer, S.-M. Ahn, E. Martinez, and G. S. D. Beach, *Nat. Mater.* **12**, 611 (2013).
- S.-H. Yang, K.-S. Ryu, and S. Parkin, *Nat. Nanotechnol.* **10**, 221 (2015).
- S.-H. Yang and S. Parkin, *J. Phys. Condens. Matter* **29**, 303001 (2017).
- R. Bläsing, T. Ma, S.-H. Yang, C. Garg, F. K. Dejene, A. T. N'Diaye, G. Chen, K. Liu, and S. S. P. Parkin, *Nat. Commun.* **9**, 4984 (2018).
- M. Hayashi, L. Thomas, C. Rettner, R. Moriya, Y. B. Bazaliy, and S. S. P. Parkin, *Phys. Rev. Lett.* **98**, 037204 (2007).
- L. Thomas, S.-H. Yang, K.-S. Ryu, B. Hughes, C. Rettner, D.-S. Wang, C.-H. Tsai, K.-H. Shen, and S. S. P. Parkin, in *2011 International Electron Devices Meeting (IEEE, 2011)*, pp. 24.2.1–24.2.4.
- A. Hoffmann, *IEEE Trans. Magn.* **49**, 5172 (2013).
- J. Sinova, S. O. Valenzuela, J. Wunderlich, C. H. Back, and T. Jungwirth, *Rev. Mod. Phys.* **87**, 1213 (2015).
- I. Dzyaloshinsky, *J. Phys. Chem. Solids* **4**, 241 (1958).
- T. Moriya, *Phys. Rev.* **120**, 91 (1960).
- L. Liu, C.-F. Pai, Y. Li, H. W. Tseng, D. C. Ralph, and R. A. Buhrman, *Science* **336**, 555 (2012).
- A. V. Khvalkovskiy, V. Cros, D. Apalkov, V. Nikitin, M. Krounbi, K. A. Zvezdin, A. Anane, J. Grollier, and A. Fert, *Phys. Rev. B* **87**, 020402 (2013).
- A. N. Bogdanov and U. K. Röfler, *Phys. Rev. Lett.* **87**, 037203 (2001).
- K.-S. Ryu, S.-H. Yang, L. Thomas, and S. S. P. Parkin, *Nat. Commun.* **5**, 3910 (2014).
- C. O. Avci, E. Rosenberg, L. Caretta, F. Büttner, M. Mann, C. Marcus, D. Bono, C. A. Ross, and G. S. D. Beach, *Nat. Nanotechnol.* **14**, 561 (2019).
- L. Caretta, M. Mann, F. Büttner, K. Ueda, B. Pfau, C. M. Günther, P. Hession, A. Churikova, C. Klose, M. Schneider, D. Engel, C. Marcus, D. Bono, K. Bagschik, S. Eisebitt, and G. S. D. Beach, *Nat. Nanotechnol.* **13**, 1154 (2018).
- K. Cai, Z. Zhu, J. M. Lee, R. Mishra, L. Ren, S. D. Pollard, P. He, G. Liang, K. L. Teo, and H. Yang, *Nat. Electron.* **3**, 37 (2020).
- S. S. P. Parkin, N. More, and K. P. Roche, *Phys. Rev. Lett.* **64**, 2304 (1990).
- P. J. H. Bloemen, H. W. van Kesteren, H. J. M. Swagten, and W. J. M. de Jonge, *Phys. Rev. B* **50**, 13505 (1994).
- S. S. P. Parkin, *Phys. Rev. Lett.* **67**, 3598 (1991).
- K.-S. Ryu, S.-H. Yang, and S. Parkin, *New J. Phys.* **18**, 053027 (2016).
- T. Tanaka, H. Kontani, M. Naito, T. Naito, D. S. Hirashima, K. Yamada, and J. Inoue, *Phys. Rev. B* **77**, 165117 (2008).